Research Square

Preprints are preliminary reports that have not undergone peer review.
They should not be considered conclusive, used to inform clinical practice,
or referenced by the media as validated information.

Design and In Silico Evaluation of Organometallic-Enhanced Chromone- Thiazole Hybrid Antioxidants: A DFT Investigation of HAT/SPLET Mechanism Switching and Solvent-Corrected Radical Scavenging Thermodynamics

Frans Augusthinus Asmuruf

frans.asmuruf@fmipa.uncen.ac.id

Cenderawasih University

Yohanis Irenius Mandik

Cenderawasih University

Jonathan Kiwasi Wororomi

Cenderawasih University

Eva Susanty Simaremare

Cenderawasih University

Research Article

Keywords: chromone-thiazole hybrid, antioxidant mechanism, HAT, SPLET, SET-PT, Q-Chem, SMD, organometallic enhancement, solvated proton, solvated electron

Posted Date: June 2nd, 2026

DOI: https://doi.org/10.21203/rs.3.rs-9768974/v1

License: This work is licensed under a Creative Commons Attribution 4.0 International License.
Read Full License

Additional Declarations: No competing interests reported.

Version of Record: A version of this preprint was published at Journal of Molecular Modeling on August 12th, 2026. See the published version at https://doi.org/10.1007/s00894-026-06887-1.

Abstract

Context:

Chromone- and thiazole-containing scaffolds are compact antioxidant and drug-design motifs, yet the extent to which organometallic modification can redirect their radical-scavenging pathways remains insufficiently resolved. In particular, systematic Q-Chem-based evaluation of hydrogen atom transfer (HAT), sequential proton-loss electron transfer (SPLET), and single-electron transfer followed by proton transfer (SET-PT) for chromone-thiazole hybrids is still limited. This study addresses that gap by designing HCT base, MeO-HCT, NO_2-HCT, HCT-$CuCl_2$, and HCT-$ZnCl_2$ models and testing whether substituent effects and metal coordination promote solvent-dependent switching between HAT/SPLET mechanisms.

Methods

Geometry optimizations and harmonic frequency calculations were performed using omega B97X-D/def2-SVP, followed by single-point SMD calculations at omegaB97X-D/def2-TZVP in water, methanol, ethanol, DMSO, and trichloromethane. Neutral ArOH, HAT radical ArO*, SPLET anion ArO^-, SET-PT radical cation $ArOH^{*+}$, and Cu spin-coupling candidates were evaluated. Thermochemical corrections from the frequency calculations were combined with solvent-specific H^+ and e^- carrier conventions to obtain BDE, IP, PDE, PA, and ETE descriptors. The originally incomplete solvent calculations were re-run and integrated into the final audit. The merged reanalysis contained 219 raw SMD single-point blocks, including superseded failed attempts; after duplicate resolution, 208 unique system-state-solvent records were successful, and no unresolved solvent single-point failure remained for descriptor construction. The results show that gas-phase descriptors favor HAT, whereas polar solvents markedly stabilize proton-loss terms, making SPLET competitive or dominant in several systems. Electron-donating MeO substitution facilitates radical stabilization, NO2 substitution perturbs charge-separation energetics, and Cu/Zn coordination modulates both descriptor ordering and convergence sensitivity. These findings establish a compact in silico framework for solvent-aware design of organometallic-enhanced chromone-thiazole antioxidants.

1 Introduction

The computational design of antioxidants has shifted from simple ranking of hydrogen-donating ability toward mechanism-resolved evaluation of radical scavenging in realistic media. A phenolic or heteroaromatic antioxidant can react through direct hydrogen atom transfer (HAT), sequential electron transfer-proton transfer (SET-PT), or sequential proton-loss electron transfer (SPLET). These mechanisms are commonly summarized by the bond dissociation enthalpy/free energy (BDE), ionization potential (IP), proton dissociation enthalpy (PDE), proton affinity (PA), and electron transfer enthalpy/free energy (ETE) descriptors [1–3]. However, recent critical discussions have emphasized that these

descriptors are not independent; the thermodynamic cycles of SET-PT and SPLET must obey energy-conservation identities, and mechanistic assignment is not meaningful unless the medium, ion conventions, and reference species are treated consistently [2, 3].

Chromone is a privileged oxygen-containing scaffold in medicinal chemistry, while thiazole-containing polyphenolic and heteroaromatic derivatives have recently shown promising antioxidant, antiradical, and biological activity profiles [10–12]. Hybridization of these motifs is therefore chemically appealing: the chromone subunit supplies conjugated carbonyl/phenoxy stabilization, whereas thiazole introduces N/S heteroatoms able to tune electron density, coordination, and intermolecular recognition. Yet the specific combination of a compact hydroxychromone-thiazole hybrid with organometallic $CuCl_2$/$ZnCl_2$ modulation has not been systematically explored as a small, DFT-tractable platform for radical-scavenging design.

A second unresolved issue is the role of the solvent in switching antioxidant mechanisms. Gas-phase calculations often rank HAT as the most accessible first step because O-H cleavage produces a neutral radical and a neutral H atom. In polar solvents, SPLET can become competitive or dominant because deprotonation is strongly stabilized by the medium. A rigorous SPLET/SET-PT comparison in solution, therefore, requires explicit inclusion of solvated H^+ and e^- reference constants rather than merely comparing molecular SMD energies [3, 4]. This point is not a minor numerical adjustment; it can invert mechanistic ranking and is essential for any claim of solvent-driven HAT/SPLET switching.

The present work addresses these gaps through a Q-Chem-based DFT workflow applied to HCT base, MeO-HCT, NO_2-HCT, and $CuCl_2$/$ZnCl_2$-enhanced analogues. The novelty is fourfold. First, it proposes a compact, Q-Chem-executable antioxidant dataset that is small enough for routine frequency and solvent validation but chemically rich enough to probe substituent and metal effects. Second, it explicitly distinguishes raw apparent SMD descriptors from solvent-corrected absolute descriptors containing H^+ and e^- solvation constants. Third, it evaluates spin-coupling candidates for Cu-containing open-shell states instead of assuming a single spin solution. Fourth, it demonstrates that organometallic enhancement and solvent polarity do not act independently: metals influence intrinsic BDE/PA trends, while polar solvents determine whether HAT or SPLET is thermodynamically preferred. This combination provides a mechanism-centered design map for small chromone-thiazole antioxidants suitable for further NCI, QTAIM, NBO, docking, and experimental validation.

2 Computational methods

2.1 Molecular systems and electronic states

The investigated series comprised HCT base, MeO-HCT, NO_2-HCT, HCT-$CuCl_2$, HCT-$ZnCl_2$, and available substituted metal complexes generated during the same workflow. Four mechanistic states were treated where output data were available: neutral ArOH, HAT radical ArO*, SPLET anion ArO^-, and SET-PT radical cation $ArOH^{*+}$. For Cu-containing systems, multiple spin-coupling candidates were evaluated for the

radical and cation states, and the lowest Gibbs-energy spin solution was selected for descriptor construction. $ZnCl_2$ systems were treated as closed-shell parent complexes and open-shell charge/radical derivatives where appropriate.

2.2 Electronic-structure protocol

All calculations were carried out using Q-Chem. Gas-phase geometry optimizations and harmonic frequency calculations were performed using omegaB97X-D/def2-SVP. The omegaB97X-D functional was selected because it includes long-range corrections and empirical dispersion, which are appropriate for charge-transfer-prone and non-covalently stabilized molecular systems [5]. Def2-SVP and def2-TZVP basis sets were used as balanced split-valence and triple-zeta basis families [6]. Final solvent single-point energies were computed at omegaB97X-D/def2-TZVP with the SMD continuum solvation model [7]. SMD calculations were conducted in water, methanol, ethanol, DMSO, and trichloromethane. Molecular wavefunction and topology extensions, where required in subsequent supporting analyses, are compatible with Multiwfn/NCI workflows [8, 13].

2.3 Thermochemical descriptor definitions

Thermal enthalpy and Gibbs corrections were taken from the gas-phase frequency jobs at 298.15 K and 1 atm and added to both gas-phase and SMD single-point electronic energies. For a molecular species X, $H(X) = E_{elec}(X) + H_{corr}(X)$ and $G(X) = E_{elec}(X) + G_{corr}(X)$, where G_{corr} includes the thermal enthalpy correction and entropy term from the frequency calculation. The antioxidant descriptors were defined as follows:

$$BDE = G(ArO^*) + G(H^*) - G(ArOH)$$

$$IP = G(ArOH^{*+}) + G(e^-) - G(ArOH)$$

$$PDE = G(ArO^*) + G(H^+) - G(ArOH^{*+})$$

$$PA = G(ArO^-) + G(H^+) - G(ArOH)$$

$$ETE = G(ArO^*) + G(e^-) - G(ArO^-)$$

The same formulas were used for enthalpy descriptors. The equality IP + PDE = PA + ETE was monitored as a thermodynamic consistency check, following energy-conservation constraints for SET-PT and SPLET cycles [2].

2.4 Solvated H^+ and e^- conventions

For solvent-phase SET-PT/SPLET analysis, solvated carrier terms were introduced according to $H(H^+_{sol}) = H(H^+_{gas}) + \Delta H_{sol}(H^+)$ and $G(H^+_{sol}) = G(H^+_{gas}) + \Delta G_{sol}(H^+)$; analogous expressions were used for e^-. Solvation constants were taken from solvent-specific literature conventions for the proton and electron [3, 4]. Water, methanol, ethanol, and DMSO were treated as supported solvents. Trichloromethane was

retained for HAT/BDE comparison but excluded from absolute SET-PT/SPLET ranking because the protonated-solvent convention is not robust in the available cluster-continuum treatment. The solvent-carrier constants are summarized in Table 1, which should appear immediately below this paragraph.

[Insert Table 1 here]

Table 1
Solvated carrier constants used for absolute solvent-phase SET-PT/SPLET descriptors. Trichloromethane was not used for absolute H^+/e^- ranking.

Solvent	Q-Chem name	$\Delta G_{sol}(H^+)$ kcal mol^{-1}	$\Delta G_{sol}(e^-)$ kcal mol^{-1}	Use in ranking
water	water	-238.0	-32.5	supported
methanol	methanol	-243.0	-27.2	supported
ethanol	ethanol	-244.4	-25.6	supported
dmso	dmso	-262.4	-20.2	supported
trichloromethane	trichloromethane	n/a	n/a	HAT-only

3 Results and discussion

3.1 Data integrity, convergence, and thermochemical audit

The original dataset contained 50 Q-Chem output files and 214 detected SMD single-point blocks. The solvent jobs that were previously classified as failed or partial were re-run and supplied as replacement outputs for HCT base HAT/methanol, HCT-$CuCl_2$ HAT/methanol, HCT-$CuCl_2$ SPLET/water, HCT-$ZnCl_2$ HAT/water, MeO-HCT HAT/DMSO-trichloromethane, and NO2-HCT-$ZnCl_2$ neutral/methanol-DMSO. Incorporating these repaired outputs increased the raw audit to 219 detected SMD blocks. Only eight failed blocks remain as superseded historical attempts; every failed key now has a converged replacement. The final deduplicated descriptor matrix, therefore, contains 208 unique successful system-state-solvent single-point records and 0 unresolved solvent single-point failures. Frequency thermochemistry remains available for 42 molecular states and was used consistently for enthalpy and Gibbs corrections. This revised audit strengthens the solvent-dependent mechanism analysis because methanol, water, and DMSO descriptors are no longer inferred from incomplete or surrogate solvent rows. The computational audit is summarized in Table 2, which should appear immediately below this paragraph.

[Insert Table 2 here]

Table 2
Computational audit summary for the Q-Chem output dataset.

Metric	Value	Interpretation
Original output files audited	50	Initial HCT, MeO-HCT, NO2-HCT, CuCl2, and ZnCl2 output files
Repair/replacement solvent outputs	6	Previously failed solvent single-point jobs were re-run and integrated
Raw detected SMD SP blocks after repair	219	Includes superseded failed attempts and newly converged replacement jobs
Raw successful SP blocks after repair	211	All successful raw blocks retained for traceability before duplicate resolution
Final deduplicated usable SP records	208	Unique system-state-spin-solvent records used for descriptor construction
Unresolved failed/partial SP records	0	All earlier failed solvent keys have converged replacements
Frequency thermochemistry rows	42	Used for enthalpy/Gibbs corrections
Imaginary-frequency caution	NO_2-HCT-$CuCl_2$ SPLET anion has 1 imaginary frequency	Descriptors retained with lower confidence and flagged for reoptimization

3.2 Optimized structural motifs and metal coordination

The parent organic structures preserve the intended chromone-thiazole framework: a conjugated chromone-like oxygenated core connected to a thiazole N/S heterocycle. The metal derivatives show coordination geometries that are chemically distinct between $CuCl_2$ and $ZnCl_2$. In HCT-$ZnCl_2$, Zn is coordinated near the thiazole N and oxygen donor region, with Zn-N and Zn-O contacts of approximately 2.13 and 2.31 Å in the parent HCT complex. Cu-containing complexes show stronger spin sensitivity and, depending on substituent pattern, can localize closer to heteroatom-rich regions or polar substituent sites. The NO_2-HCT metal complexes, for example, place Cu/Zn near nitro/oxygen donors, indicating that substituent electronics can redirect metal-ligand organization. This structural flexibility provides the non-covalent/coordination basis for metal-dependent radical and proton-loss descriptors.

[Insert Fig. 1 here]

Figure 1 Representative optimized structures of HCT base, MeO-HCT, NO_2-HCT, HCT-$CuCl_2$, and HCT-$ZnCl_2$ from the Q-Chem geometry-optimization dataset. Atom colors follow standard molecular-rendering conventions.

3.3 Gas-phase descriptors: HAT dominates before single-ion solvation correction

Gas-phase Gibbs descriptors show a clear thermodynamic preference for HAT as the first radical-scavenging step. Organic substitution follows chemically reasonable trends: MeO-HCT lowers BDE relative to HCT base, whereas NO_2-HCT increases BDE. The parent HCT-$CuCl_2$ complex is the strongest gas-phase HAT enhancer in the dataset, decreasing BDE(G) from 78.6 kcal mol^{-1} for HCT base to 56.4 kcal mol^{-1}. HCT-$ZnCl_2$ gives a BDE close to the parent organic ligand, but it markedly reduces PA relative to the HCT base, indicating that Zn coordination primarily affects deprotonation rather than neutral O-H homolysis. This contrast between Cu and Zn is important: Cu can stabilize radical character and open-shell states, whereas Zn acts more as a Lewis-acidic polarizer of the anionic/deprotonated channel. The gas-phase descriptor values are summarized in Table 3, which should appear immediately below this paragraph, and the corresponding graphical comparison is shown in Fig. 2, which should appear immediately after Table 3.

[Insert Table 3 here]

Table 3

Gas-phase Gibbs descriptors in kcal mol^{-1}. HAT is the lowest first-step descriptor for all fully validated gas-phase systems.

System	BDE(G) HAT	IP(G) SET-PT	PA(G) SPLET	Preferred gas first step
HCT base	78.6	176.3	336.7	HAT
HCT-CuCl2	56.4	190.2	299.6	HAT
HCT-ZnCl2	78.2	198.4	302.9	HAT
MeO-HCT	75.6	174.7	332.9	HAT
MeO-HCT-CuCl2	77.3	193.2	321.6	HAT
MeO-HCT-ZnCl2	78.4	184.2	334.1	HAT
NO2-HCT	82.4	184.9	330.0	HAT
NO2-HCT-ZnCl2	82.9	190.7	299.6	HAT

[Insert Fig. 2 here]

Figure 2 Gas-phase thermochemically corrected first-step descriptors. The much lower BDE values relative to IP and PA explain why HAT dominates before solvent-specific single-ion corrections are introduced.

3.4 Solvent-corrected descriptors: HAT-to-SPLET switching

The central mechanistic result emerges only after solvent-specific H + and e^- constants are included. The repaired solvent outputs complete the previously missing methanol, water, and DMSO entries and confirm that PA(G) is lower than BDE(G) for every supported system-solvent combination in water, methanol, ethanol, and DMSO. This reverses the gas-phase ranking and identifies SPLET, not HAT, as the thermodynamically most accessible first step in polar media. The completed methanol row for HCT base gives BDE(G) = 75.34 kcal mol-1 and PA(G) = 43.01 kcal mol^{-1}, consistent with water and ethanol and confirming that the SPLET preference is not an artefact of missing methanol data. The completed water row for HCT-$CuCl_2$ gives BDE(G) = 56.81 kcal mol^{-1} and PA(G) = 22.71 kcal mol^{-1}, while the completed DMSO row for MeO-HCT gives BDE(G) = 72.87 kcal mol^{-1} and PA(G) = 26.33 kcal mol^{-1}. DMSO consistently produces the lowest PA(G) values because proton-loss stabilization is strongest under the adopted single-ion convention. This behaviour is consistent with the broader consensus that polar solvents can promote deprotonation-controlled antioxidant pathways, whereas non-polar media preserve a more HAT-like thermodynamic picture [1–4]. The solvent-corrected descriptor summary is given in Table 4, which should appear immediately below this paragraph; the PA heatmap and the BDE-PA switching gap are shown in Fig. 3 and Fig. 4, respectively, which should appear immediately after Table 4.

[Insert Table 4 here]

Table 4
Summary of solvent-corrected Gibbs descriptors. The positive BDE-PA gap indicates that PA lies below BDE and that SPLET is favoured as the first step in supported polar solvents.

System	Lowest BDE(G) solvent	Lowest BDE(G)	Lowest PA(G) solvent	Lowest PA(G)	BDE-PA gap	Solvent ranking
HCT base	water	74.6	dmso	29.3	45.3	SPLET(PA)
MeO-HCT	dmso	72.9	dmso	26.3	46.5	SPLET(PA)
NO2-HCT	water	76.9	dmso	28.8	48.1	SPLET(PA)
HCT-CuCl2	dmso	53.2	dmso	-0.6	53.8	SPLET(PA)
HCT-ZnCl2	dmso	74.6	dmso	2.5	72.1	SPLET(PA)
MeO-HCT-CuCl2	dmso	74.9	dmso	19.3	55.6	SPLET(PA)
MeO-HCT-ZnCl2	dmso	77.6	dmso	36.7	40.9	SPLET(PA)
NO2-HCT-CuCl2	water	75.0	dmso	10.3	64.7	SPLET(PA)
NO2-HCT-ZnCl2	water	76.5	dmso	2.9	73.6	SPLET(PA)

[Insert Fig. 3 here]

Fig. 3 Heatmap of PA(G) values after solvent-specific H^+ correction. Lower PA values indicate easier first-step deprotonation and stronger SPLET accessibility.

[Insert Fig. 4 here]

Figure 4 Mechanistic switching gap, BDE(G) – PA(G). Positive values indicate that SPLET is thermodynamically lower than HAT for the first step. DMSO produces the largest switching gaps.

3.5 Organometallic enhancement and substituent effects

The organometallic contribution is not uniform and cannot be reduced to a single 'metal improves antioxidant activity' statement. In the gas phase, HCT-CuCl2 gives a pronounced HAT enhancement, but MeO-HCT-CuCl2 does not show the same BDE decrease, emphasizing that metal coordination geometry and substituent placement jointly determine radical stabilization. The repaired HCT-CuCl2 HAT/methanol calculation is particularly important because it replaces the earlier incomplete m3 solvent job and confirms that the selected low-energy m3 radical solution gives a methanol BDE(G) of 55.75 kcal mol-1, close to ethanol and DMSO, and much lower than organic HCT. ZnCl2 derivatives often show more striking effects on PA than on BDE. For example, DMSO PA(G) decreases from 29.28 kcal mol-1 for HCT base to 2.47 kcal mol-1 for HCT-ZnCl2 and to 2.85 kcal mol-1 for NO2-HCT-ZnCl2 after the repaired NO2-HCT-ZnCl2 neutral methanol/DMSO outputs are included. HCT-CuCl2 remains even more extreme, with DMSO PA(G) slightly negative (-0.60 kcal mol-1) under the chosen convention, indicating near barrierless thermodynamic access to the deprotonated state, although kinetic and explicit-solvent validation would be needed before translating this into reaction-rate claims. The solvent-dependent HAT trend is summarized in Fig. 5, which should appear immediately after this paragraph.

[Insert Fig. 5 here]

Figure 5 Solvent-dependent HAT BDE(G) descriptors. Metal and substituent effects alter the intrinsic HAT scale, but solvent-corrected PA remains the decisive first-step discriminator in polar media.

3.6 Cu spin-coupling candidates

Cu-containing systems require explicit spin-coupling screening. For HCT-CuCl2 HAT radical, the m3 solution is lower than m1 by 16.92 kcal mol^{-1}, whereas for the SET-PT cation, the m1 solution is lower than m3 by 2.86 kcal mol^{-1}. MeO-HCT-$CuCl_2$ follows a similar pattern for the HAT radical, with m3 below m1 by 17.60 kcal mol^{-1}. These differences are too large to ignore and justify state-specific spin selection before computing antioxidant descriptors. The NO_2-HCT-$CuCl_2$ dataset is more delicate because the SPLET anion retained one imaginary frequency; its solvent descriptors are useful for trend exploration but should be reoptimized before being treated as final publication-quality energetic evidence. The Cu spin-coupling candidates are summarized in Table 5, which should appear immediately below this paragraph.

[Insert Table 5 here]

Table 5
Cu spin-coupling candidates from gas-phase Gibbs energies. Values are in kcal mol^{-1} relative to the lowest spin solution within each state.

System	State	Spin tag	ΔG vs lowest
HCT-CuCl2	HAT radical ArO	m3	0.00
HCT-CuCl2	HAT radical ArO	m1	16.92
HCT-CuCl2	SETPT radical cation ArOH plus	m1	0.00
HCT-CuCl2	SETPT radical cation ArOH plus	m3	2.86
MeO-HCT-CuCl2	HAT radical ArO	m3	0.00
MeO-HCT-CuCl2	HAT radical ArO	m1	17.60
MeO-HCT-CuCl2	SETPT radical cation ArOH plus	m3	0.00
MeO-HCT-CuCl2	SETPT radical cation ArOH plus	m1	6.20
NO2-HCT-CuCl2	HAT radical ArO	m3	0.00
NO2-HCT-CuCl2	HAT radical ArO	m1	22.46
NO2-HCT-CuCl2	SETPT radical cation ArOH plus	m3	0.00
NO2-HCT-CuCl2	SETPT radical cation ArOH plus	m1	22.83

3.7 Repaired solvent jobs, residual cautions, and limitations

The reanalysis changes the dataset status from partially complete to descriptor-complete for the supported solvent matrix. The eight historical failed blocks are retained only as a reproducibility trail because each failed key now has a converged replacement in the repaired output set. Consequently, failed solvent single-point rows are no longer excluded from descriptor construction; instead, the replacement energies are used in the final descriptor matrix. Trichloromethane remains excluded from absolute SET-PT/SPLET ranking because the adopted H+/e- carrier convention is unsupported for this solvent; it is therefore used only for HAT-like comparisons and qualitative non-polar solvent discussion. Finally, while the present work discusses non-covalent and coordination dynamics through optimized structures, metal-ligand contacts, and solvent-dependent descriptor shifts, explicit RDG/NCI maps, QTAIM bond critical points, and NBO donor-acceptor analyses should be added as Supporting Information when wavefunction files are generated. This careful separation prevents overinterpretation of thermodynamic descriptors as kinetic or topological proof.

Table 6
Repaired solvent single-point calculations incorporated into the final descriptor matrix.

System	State/solvent repaired	Final E(SMD) Eh	Effect on final descriptor matrix
HCT base	HAT radical / methanol	-1139.48530940	Completes HCT base methanol: BDE(G) 75.34; PA(G) 43.01
HCT-$CuCl_2$	HAT radical m3 / methanol	-3700.57541558	Replaces failed selected-spin m3 job: BDE(G) 55.75; PA(G) 19.70
HCT-$CuCl_2$	SPLET anion / water	-3700.73887542	Completes water SPLET descriptor: BDE(G) 56.81; PA(G) 22.71
HCT-$ZnCl_2$	HAT radical / water	-3839.49731374	Confirms water HAT descriptor: BDE(G) 75.52; PA(G) 24.91
MeO-HCT	HAT radical / DMSO	-1254.02195618	Completes DMSO HAT descriptor: BDE(G) 72.87; PA(G) 26.33
MeO-HCT	HAT radical / trichloromethane	-1254.02019985	Completes HAT-only non-polar comparison: BDE(G) 74.30
NO2-HCT-$ZnCl_2$	neutral / methanol	-4044.66529724	Completes methanol matrix: BDE(G) 77.54; PA(G) 21.28
NO2-HCT-$ZnCl_2$	neutral / DMSO	-4044.66460404	Completes DMSO matrix: BDE(G) 77.47; PA(G) 2.85

4 Conclusions

A thermochemically corrected Q-Chem DFT workflow was finalized for compact chromone-thiazole antioxidant candidates and their $CuCl_2$/$ZnCl_2$-enhanced analogues. The repaired solvent single-point calculations remove the earlier methanol, water, and DMSO gaps and yield a fully deduplicated solvent descriptor matrix for the supported polar solvents. The gas-phase results show HAT as the preferred first step, with parent HCT-$CuCl_2$ providing the strongest BDE lowering. After solvent-specific H^+ and e^- constants are incorporated, polar solvents induce a robust HAT-to-SPLET thermodynamic switch, with PA becoming lower than BDE in all supported solvent cases. DMSO gives the strongest SPLET stabilization, and metal coordination amplifies this effect most clearly for HCT-$CuCl_2$, HCT-$ZnCl_2$, NO_2-HCT-$CuCl_2$, and NO_2-HCT-$ZnCl_2$. The study provides a reproducible small-system platform for organometallic antioxidant design and highlights three methodological requirements for credible mechanism claims: frequency-validated geometries, spin-coupling screening for open-shell Cu species, and explicit single-ion solvation conventions. The most promising next steps are explicit radical reaction calculations, RDG/NCI/QTAIM/NBO analyses of the optimized structures, and experimental validation through DPPH/ABTS/ORAC assays and metal-binding spectroscopy.

Declarations

Supplementary information

The complete worksheet contains the audit table, repaired solvent single-point energies, thermochemistry, gas descriptors, apparent SMD descriptors, solvated carrier constants, absolute solvent descriptors, mechanism ranking, Cu spin-coupling comparison, and superseded failed-job log. The worksheet should be submitted as Supporting Information together with representative Q-Chem input/output files, including the repaired methanol, water, and DMSO solvent outputs reported in Table 6.

Competing interests

The author declares no competing interests.

Funding

This research received no specific grant from any funding agency in the public, commercial, or not-for-profit sectors.

Author Contribution

Frans Augusthinus Asmuruf conceived the study, performed data analysis, and wrote the initial manuscript draft. Yohanis Irenius Mandik, Jonathan Kiwasi Wororomi, and Eva Susanty Simaremare contributed to interpretation, manuscript refinement, and critical discussion. All authors reviewed and approved the final manuscript.

Acknowledgement

The author acknowledges Universitas Cenderawasih for academic support and the use of computational resources for molecular modelling and antioxidant descriptor analysis.

Data availability

All data analyzed in this manuscript were generated from the uploaded Q-Chem output files and are summarized in the accompanying worksheet. Raw Q-Chem output files and input decks can be supplied as Supporting Information upon journal submission.

References

1. Galano A, Alvarez-Idaboy JR, Francisco-Marquez M (2025) Antioxidant activity at the molecular level: exploring ways of assessing radical-scavenging mechanisms. Chem Sci.

https://doi.org/10.1039/D5SC05463J

2. Baldea I (2022) Two theorems and an important insight on how the preferred mechanism of free radical scavenging cannot be settled. Molecules 27:8092. https://doi.org/10.3390/molecules27228092
3. Markovic Z, Markovic S, Tosovic J, Milenkovic D, Markovic S (2016) Revisiting the solvation enthalpies and free energies of the proton and electron in various solvents. Comput Theor Chem 1077:11–17. https://doi.org/10.1016/j.comptc.2015.09.007
4. Tosovic J (2016) Solvation enthalpies and Gibbs energies of the proton and electron in various solvents. J Serbian Soc Comput Mech 10:72–85. https://doi.org/10.5937/jsscm1602066T
5. Chai JD, Head-Gordon M (2008) Long-range corrected hybrid density functionals with damped atom-atom dispersion corrections. Phys Chem Chem Phys 10:6615–6620. https://doi.org/10.1039/B810189B
6. Weigend F, Ahlrichs R (2005) Balanced basis sets of split valence, triple zeta valence and quadruple zeta valence quality for H to Rn: design and assessment of accuracy. Phys Chem Chem Phys 7:3297–3305. https://doi.org/10.1039/B508541A
7. Marenich AV, Cramer CJ, Truhlar DG (2009) Universal solvation model based on solute electron density and on a continuum model of the solvent defined by the bulk dielectric constant and atomic surface tensions. J Phys Chem B 113:6378–6396. https://doi.org/10.1021/jp810292n
8. Lu T, Chen F (2012) Multiwfn: a multifunctional wavefunction analyzer. J Comput Chem 33:580–592. https://doi.org/10.1002/jcc.22885
9. Shao Y, Gan Z, Epifanovsky E, Gilbert ATB, Wormit M, Kussmann J, et al (2021) Software for the frontiers of quantum chemistry: an overview of developments in the Q-Chem 5 package. J Chem Phys 155:084801. https://doi.org/10.1063/5.0055522
10. Krylov AI, Gill PMW (2013) Q-Chem: an engine for innovation. WIREs Comput Mol Sci 3:317–326. https://doi.org/10.1002/wcms.1122
11. Cornea AC, Marc G, Stana A, et al (2025) Synthesis, characterization, and antioxidant activity evaluation of new N-methyl substituted thiazole-derived polyphenolic compounds. Molecules 30:1345. https://doi.org/10.3390/molecules30061345
12. Ungureanu D, Marc G, Tiperciuc B, Moldovan C, Ionut I, Stana A, Oniga I, Vlase L, Pirnau A, Oniga O (2025) Novel 3,4-dihydroxyphenyl-thiazole-coumarin hybrid compounds: synthesis, in silico and in vitro evaluation of their antioxidant activity. Antioxidants 14:636. https://doi.org/10.3390/antiox14060636
13. Reis J, Gaspar A, Milhazes N, Borges F (2017) Chromone as a privileged scaffold in drug discovery: recent advances. J Med Chem 60:7941–7957. https://doi.org/10.1021/acs.jmedchem.6b01720
14. Wright JS, Johnson ER, DiLabio GA (2001) Predicting the activity of phenolic antioxidants: theoretical method, analysis of substituent effects, and application to major families of antioxidants. J Am Chem Soc 123:1173–1183. https://doi.org/10.1021/ja002455u

15. Johnson ER, Keinan S, Mori-Sanchez P, Contreras-Garcia J, Cohen AJ, Yang W (2010) Revealing noncovalent interactions. J Am Chem Soc 132:6498–6506. https://doi.org/10.1021/ja100936w
16. Reed AE, Curtiss LA, Weinhold F (1988) Intermolecular interactions from a natural bond orbital, donor-acceptor viewpoint. Chem Rev 88:899–926. https://doi.org/10.1021/cr00088a005
17. Bakheit AH, et al (2024) Theoretical study of the antioxidant mechanism and related molecular descriptors of bioactive compounds. Front Chem 12:1443718. https://doi.org/10.3389/fchem.2024.1443718
18. Lu XQ, et al (2023) Radical scavenging capability and mechanism of natural antioxidant candidates: a density functional theory study. Molecules/PMC dataset. https://pmc.ncbi.nlm.nih.gov/articles/PMC10343223/
19. Mardirossian N, Head-Gordon M (2017) Thirty years of density functional theory in computational chemistry: an overview and extensive assessment of 200 density functionals. Mol Phys 115:2315–2372. https://doi.org/10.1080/00268976.2017.1333644
20. Humphrey W, Dalke A, Schulten K (1996) VMD: visual molecular dynamics. J Mol Graph 14:33–38. https://doi.org/10.1016/0263-7855(96)00018-5

Figures

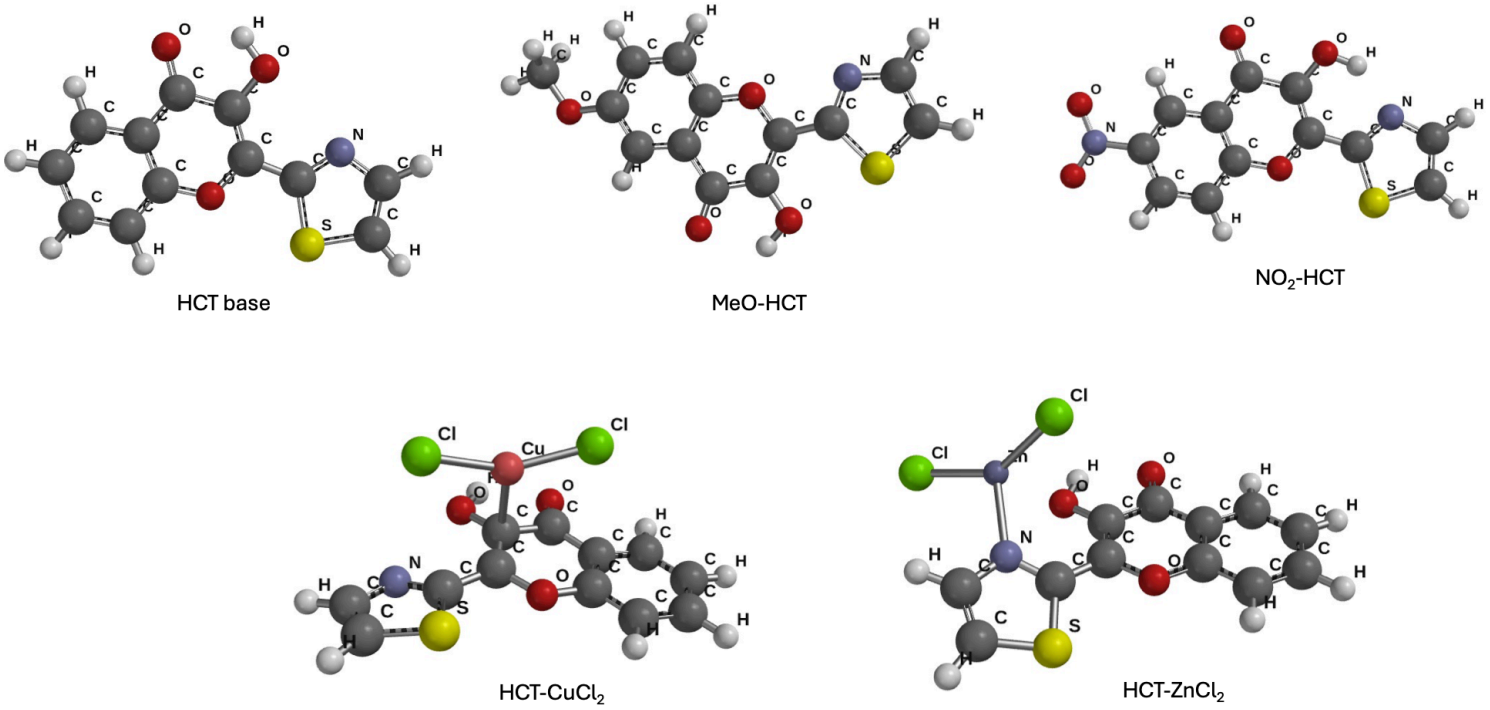

Figure 1

Representative optimized structures of HCT base, MeO-HCT, NO_2-HCT, HCT-$CuCl_2$, and HCT-$ZnCl_2$ from the Q-Chem geometry-optimization dataset. Atom colors follow standard molecular-rendering conventions.

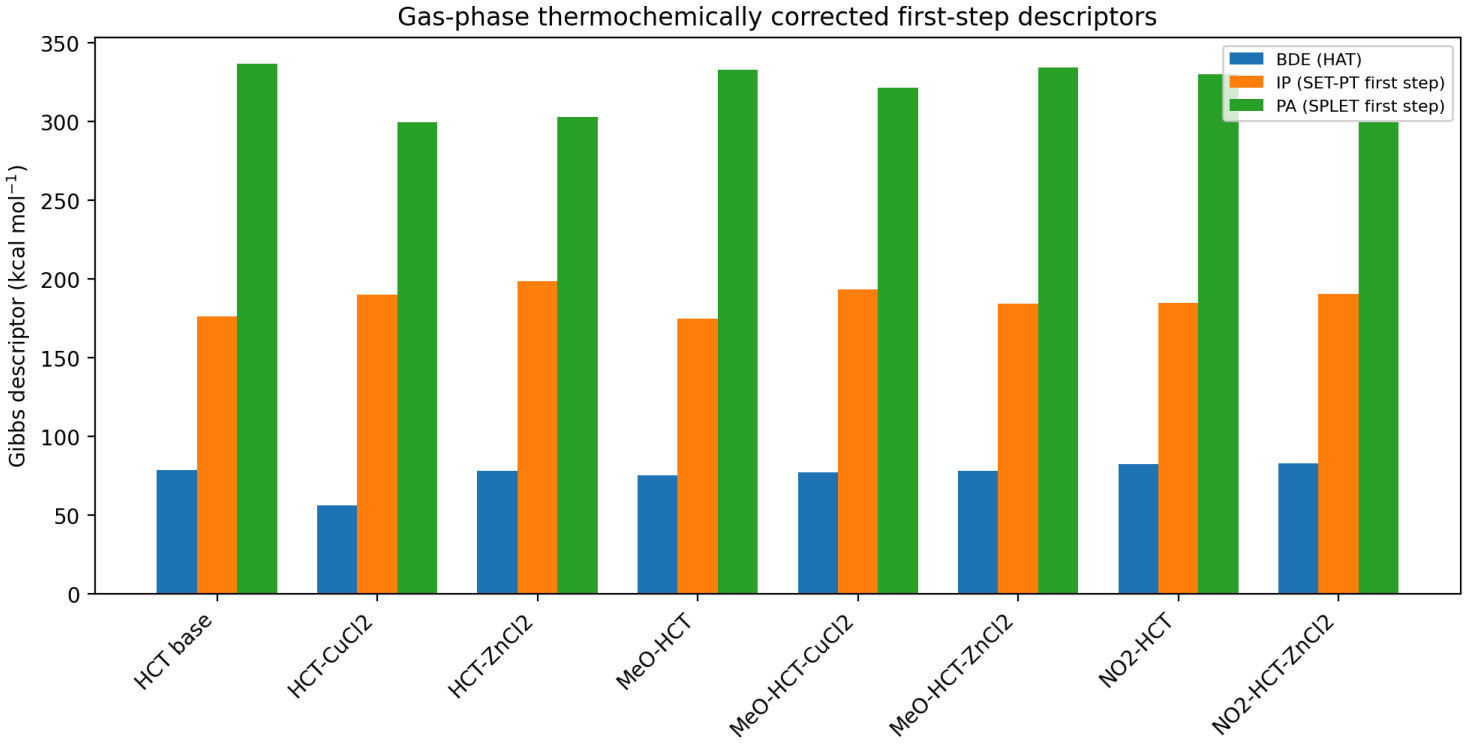

Figure 2

Gas-phase thermochemically corrected first-step descriptors. The much lower BDE values relative to IP and PA explain why HAT dominates before solvent-specific single-ion corrections are introduced.

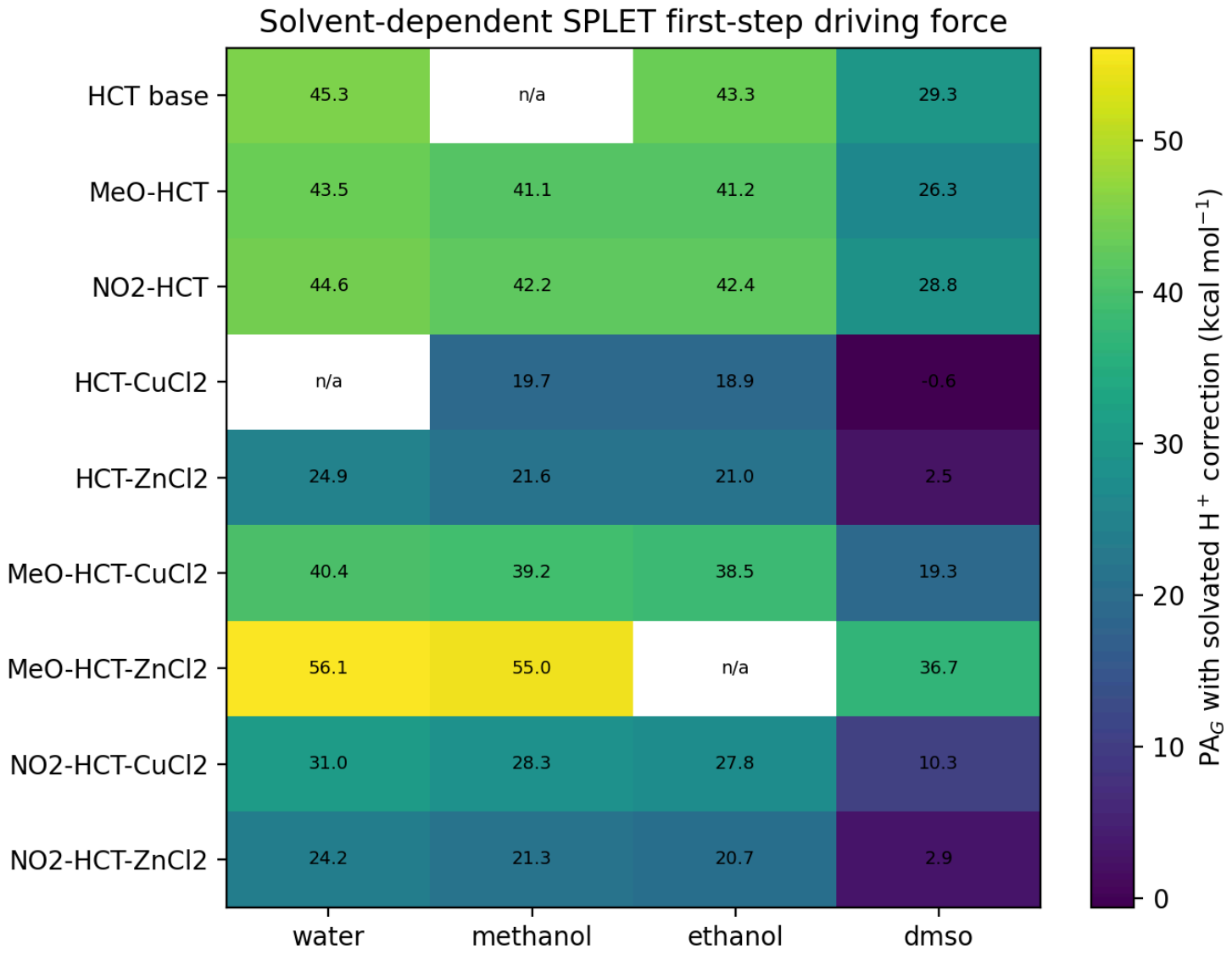

Figure 3

Heatmap of PA(G) values after solvent-specific H^+ correction. Lower PA values indicate easier first-step deprotonation and stronger SPLET accessibility.

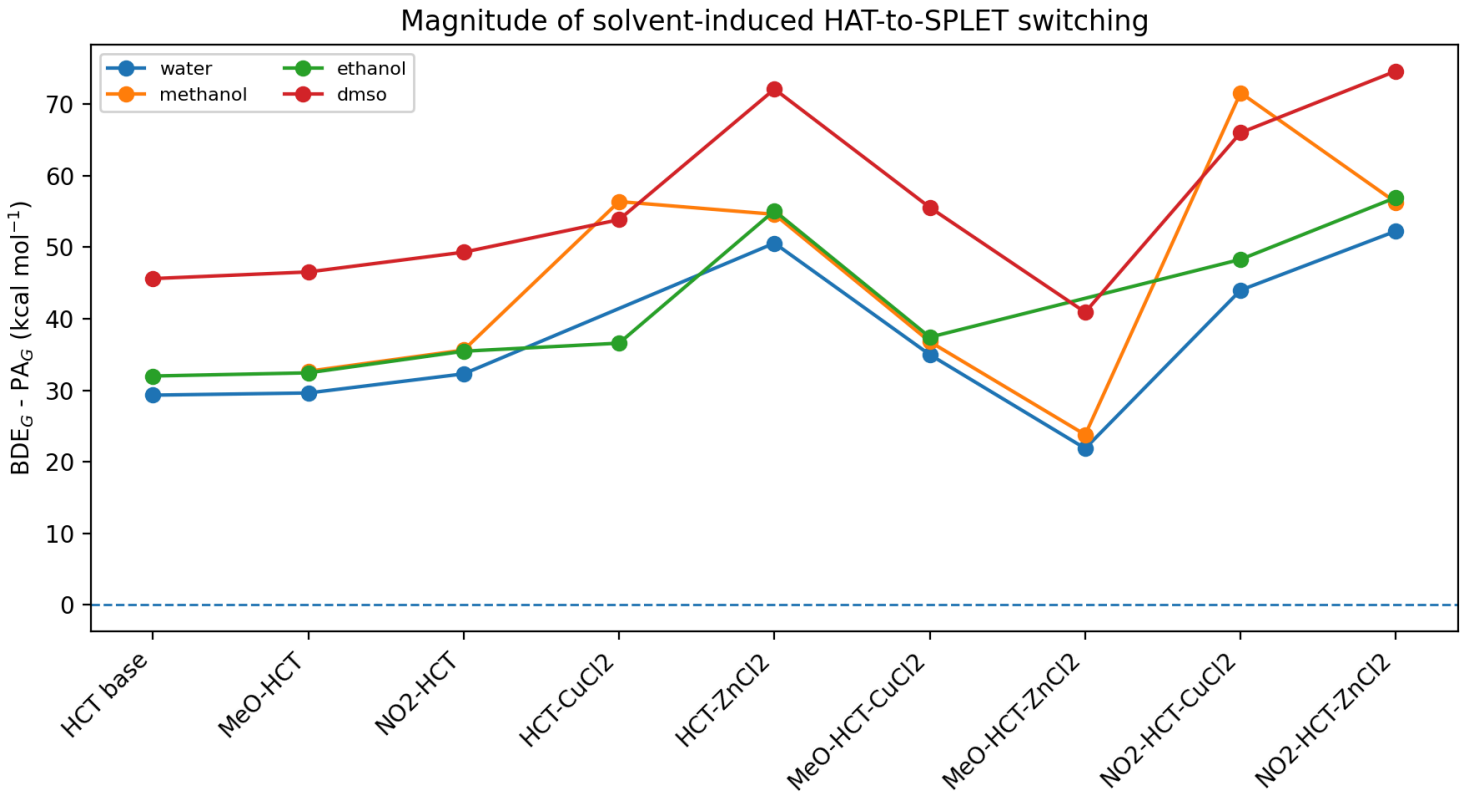

Figure 4

Mechanistic switching gap, BDE(G) – PA(G). Positive values indicate that SPLET is thermodynamically lower than HAT for the first step. DMSO produces the largest switching gaps.

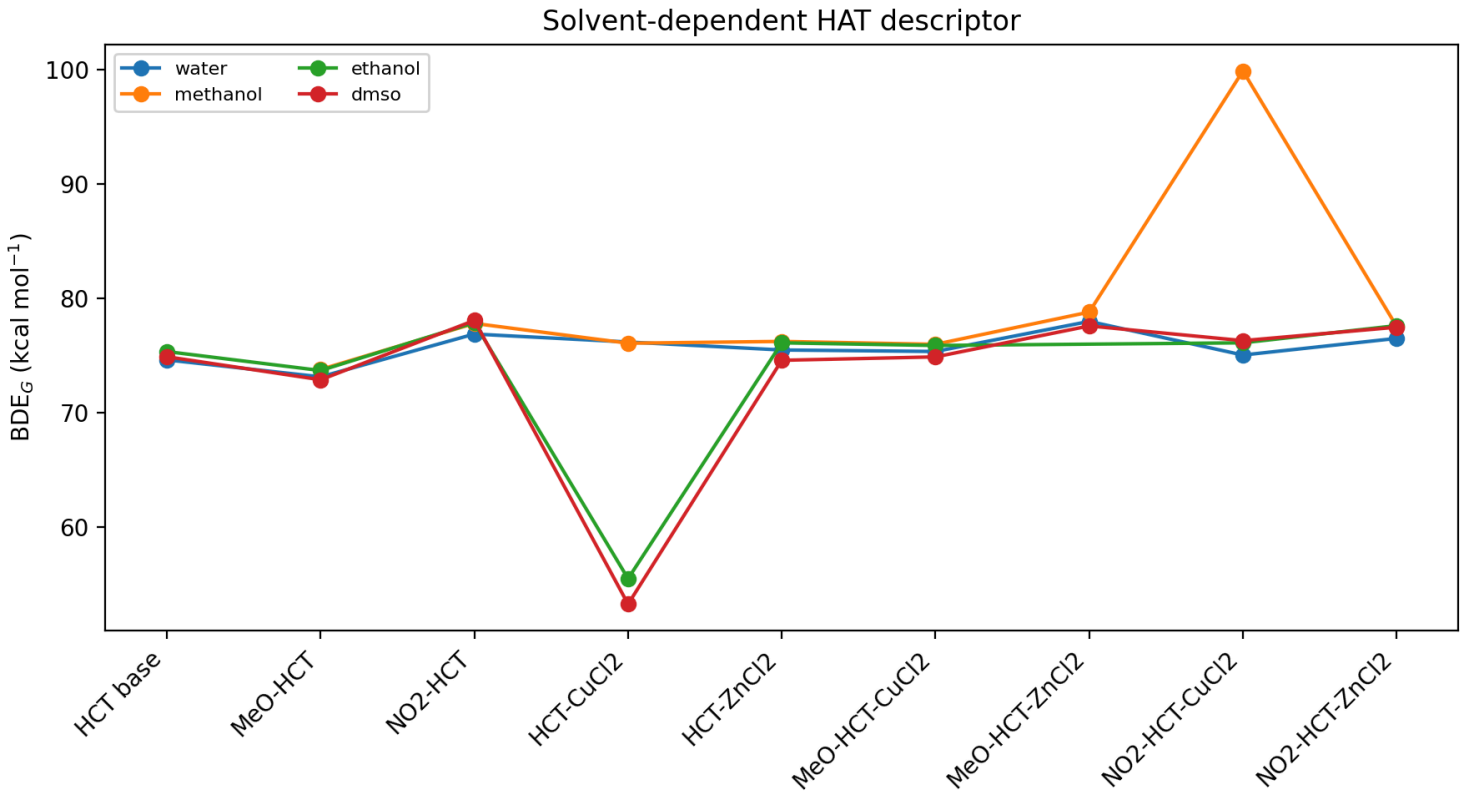

Figure 5

Solvent-dependent HAT BDE(G) descriptors. Metal and substituent effects alter the intrinsic HAT scale, but solvent-corrected PA remains the decisive first-step discriminator in polar media.